

See discussions, stats, and author profiles for this publication at: <https://www.researchgate.net/publication/223984169>

Correlation Between Molecular Conformation, Packing, and Dynamics in Oligofluorenes: A Theoretical/Experimental Study

ARTICLE in THE JOURNAL OF PHYSICAL CHEMISTRY A · APRIL 2012

Impact Factor: 2.69 · DOI: 10.1021/jp210953m · Source: PubMed

CITATIONS

11

READS

20

6 AUTHORS, INCLUDING:



Oigres D Bernardinelli

University of São Paulo

7 PUBLICATIONS 55 CITATIONS

[SEE PROFILE](#)



R. M. Faria

University of São Paulo

239 PUBLICATIONS 2,004 CITATIONS

[SEE PROFILE](#)



E. R. Deazevedo

University of São Paulo

111 PUBLICATIONS 1,668 CITATIONS

[SEE PROFILE](#)



Melissa Siqueira

Universidade Federal de Ouro Preto

11 PUBLICATIONS 36 CITATIONS

[SEE PROFILE](#)

Correlation Between Molecular Conformation, Packing, and Dynamics in Oligofluorenes: A Theoretical/Experimental Study

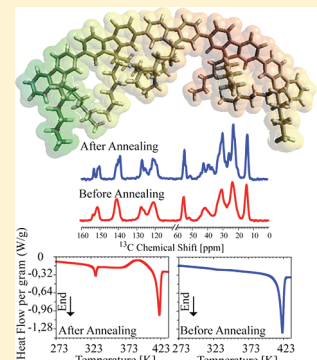
Oigres Daniel Bernardinelli,[†] Gregório Couto Faria,[†] Luiz Antonio de Oliveira Nunes,[†] Roberto Mendonça Faria,[†] Eduardo Ribeiro deAzevedo,^{*,†} and Melissa Fabíola Siqueira Pinto^{*,‡}

[†]Instituto de Física de São Carlos, Universidade de São Paulo, CP 369, 13660-970, São Carlos, SP, Brazil

[‡]Departamento de Física, Universidade Federal de Ouro Preto, Campus Universitário Morro do Cruzeiro, Ouro Preto-MG 35400-00, Ouro Preto, MG, Brazil

Supporting Information

ABSTRACT: Fluorene-based systems have shown great potential as components in organic electronics and optoelectronics (organic photovoltaics, OPVs, organic light emitting diodes, OLEDs, and organic transistors, OTFTs). These systems have drawn attention primarily because they exhibit strong blue emission associated with relatively good thermal stability. It is well-known that the electronic properties of polymers are directly related to the molecular conformations and chain packing of polymers. Here, we used three oligofluorenes (trimer, pentamer, and heptamer) as model systems to theoretically investigate the conformational properties of fluorene molecules, starting with the identification of preferred conformations. The hybrid exchange-correlation functional, OPBE, and ZINDO/S-CI showed that each oligomer exhibits a tendency to adopt a specific chain arrangement, which could be distinguished by comparing their UV-vis electronic absorption and ¹³C NMR spectra. This feature was used to identify the preferred conformation of the oligomer chains in chloroform-cast films by comparing experimental and theoretical UV-vis and ¹³C NMR spectra. Moreover, the oligomer chain packing and dynamics in the films were studied by DSC and several solid-state NMR techniques, which indicated that the phase behavior of the films may be influenced by the tendency that each oligomeric chain has to adopt a given conformation.



I. INTRODUCTION

Organic semiconductor-like materials are being used more often as active layers in electronic devices (organic photovoltaics, OPVs, organic light emitting diodes, OLEDs, and organic transistors, OTFTs) because they present novel optoelectronic properties and are easy to process.^{1–3} Among the several conjugated organic systems that have emerged and are incorporated into such devices, there are oligomers and polymers of fluorene. The fluorene family exhibits many attractive features, such as strong luminescence, blue light emission, and facile color-tuning via structural modifications.^{4–7} The electronic properties of oligo- and polyfluorenes depend, in general, on molecular arrangement and also morphology. Despite the success of their optoelectronic applications, many aspects of fluorene systems, including the nature of their chain conformations, structural phases, and effects on electro-optical properties, remain unknown. Depending on the experimental conditions of synthesis and the effective length of the chains, fluorene-based systems can exhibit different phases. Some works have demonstrated phases with amorphous features and some crystalline phases.⁸ Using Raman spectroscopy, Tsoi and Lidzey identified the β -phase (with planarized conformation) in the pentamer of fluorene, as observed for toluene-cast poly(9,9-diethylfluorene) [PF8] polymer, which also exhibits a crystalline phase with a helical conformation, referred to as the α -phase.⁹

In this work, we present molecular quantum mechanics calculations and experimental studies of three oligofluorenes with three (3F6), five (5F6), and seven (7F6) repeat units to address the correlation between the molecular conformation, packing, and dynamics of their chains. These discussions are supported by experimental optical, thermal, and NMR measurements.

II. MATERIALS AND METHODS

Theoretical Procedures. The main goal of the theoretical calculations performed in this study was to predict the most feasible chain conformation for fluorene oligomers (3F6, 5F6, and 7F6; see chemical structure in Figure 1a). To this end, each theoretical step was followed by an experimental measurement, for example, UV-vis or NMR. Initially, we sought the most stable molecular conformations. These structures were selected from conformational analysis using the MM3 molecular mechanics force field implemented in the TINKER program package.¹⁰ The structures then were fully optimized using the hybrid exchange-correlation OPBE functional, a density functional theory (DFT) approach associated with Pople's 6-31G (d,p) standard basis set. The DFT theory was chosen for

Received: November 14, 2011

Revised: March 27, 2012

Published: April 3, 2012

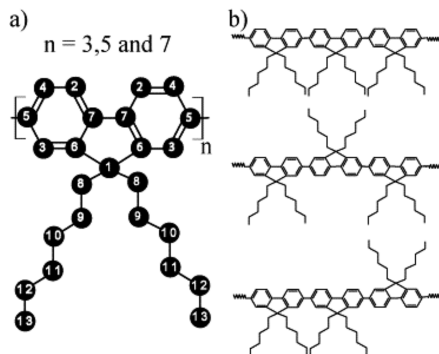


Figure 1. (a) Sketch of the chemical structure of the fluorene oligomers with the numerical index used in the assignment of the NMR spectrum. (b) Representation of the side-chain configurations considered in the theoretical calculation for the trimer (3F6). Similar side-chain configurations for the pentamer (5F6) and heptamer (7F6) were also considered in the calculation, covering other possible configurations.

its remarkable performance in ^{13}C shielding predictions^{11,12} and was also employed to predict the chemical shifts in the ^{13}C NMR spectra of fully optimized geometries of each oligomer using the GIAO (gauge-independent atomic orbital) method. The ^{13}C relative chemical shifts (δ) were calculated with respect to the absolute shielding values (σ) of tetramethylsilane (TMS), using $\delta = \sigma_{\text{ref}} - \sigma$. These calculations were performed using the Gaussian 03 program.¹³ Moreover, electronic absorption spectra were calculated using the ZINDO/S-CI approach (Zerner's Intermediate Neglect of Differential Overlap/Spectroscopic parameters), employing the electronic structure program package ORCA.^{14–16}

Sample Preparation. All oligomers were purchased from American Dye Source Co. The chemical structures are shown in Figure 1a. The oligomers 3F6, 5F6, and 7F6 have purities of 99.0% (3F6), 98.0% (5F6), and 99.0% (7F6) and molecular weights (MW) of 999.58, 1664.62, and 2327.77 g mol⁻¹, respectively. The experiments were carried out in films obtained by drop-casting from 2 mg/mL chloroform solutions. Because the goal was to investigate how the minimum-energy conformations may influence the solid-state conformations, we chose chloroform as a solvent because it is preferentially attracted by the side chains¹ and has a weaker effect on the backbone conformations as compared to the effects of other solvents, such as toluene. The films used for UV-vis measurements were deposited on quartz plates, while those used for solid-state NMR measurements were drop-cast onto a Petri disk and removed after solvent evaporation. Samples were divided into two types. One was used for ^{13}C solid-state NMR measurements as a function of temperature and the other for DSC measurements. Moreover, after the NMR experiments, the samples were thermally analyzed by DSC.

Experimental Procedures. UV-vis absorption measurements were performed in the 280–500 nm range with 5 nm resolution using a UV-vis/NIR spectrometer Perkin-Elmer Lambda 900 with 5 nm slit widths. Solid-state ^{13}C NMR experiments were carried out in a Varian Inova spectrometer at ^{13}C and ^1H frequencies of 100.5 and 400.0 MHz, respectively; and a Varian (Jackobsen design) 7 mm magic-angle spinning (MAS) double-resonance probe head was used. ^1H – ^{13}C cross-polarization with a radio frequency ramp under MAS, and ^1H two-pulse phase modulation (TPPM) decoupling, denoted here simply as CP-MAS, was used to acquire the ^{13}C solid-state

NMR spectra. All of the experiments were carried out at spinning frequencies of 5 kHz, using a cross-polarization time of 1 ms, acquisition time of 20 ms, decoupling power of 60 kHz, and recycle delay of 4 s. During a set of NMR experiments, the samples were held at a selected temperature for approximately 2 h. All measurements were conducted starting at 245 K, and the temperature was increased at a rate of 2 K/min between experiments. These maximum temperatures were 331 K for 3F6, 362 K for 5F6, and 377 K for 7F6. The samples were then cooled to room temperature using the same procedure, that is, stopping at selected temperatures for 2 h during the NMR measurements and cooling between temperatures at a rate of 2 K/min. From now on, we will refer to the samples submitted to this thermal treatment during the NMR experiments simply as treated samples.

Differential scanning calorimetry (DSC) measurements were performed for the as-cast as well as the thermally treated samples. DSC thermograms were acquired in two scans steps. The samples were cooled to 213 K and then heated at a rate of 10 K/min to 443 K. After cooling to 213 K, a second scan was carried out to verify the behavior after removing the thermal history of each sample.

WAXS experiments were performed at the SAXS1 beamline of the Brazilian Synchrotron Light Laboratory (LNLS). The wavelength used was 1.488 Å, and the sample-detector distance was approximately 189.62 mm. The sample scattering was registered using a two-dimensional MAR-CCD detector, with 5 min of data acquisition. Average radial intensity profiles were obtained by integrating an arbitrary 5° angular sector. Intensities were normalized by the integrated intensity incident on each sample during the exposure and by sample absorption. Parasitic scattering was subtracted from each pattern.

III. RESULTS

Selection of Minimum Energy Conformations. As mentioned in section II, the first step in the theoretical calculation was to seek the most stable conformations considering different side-chain configurations. For 3F6, only three side-chain arrangements seemed possible, as depicted in Figure 1b. For 5F6 and 7F6, on the other hand, several feasible arrangements were found; many of them, however, were excluded on the basis of comparisons with the experimental results (the excluded ones are presented in the Supporting Information). The corresponding molecular structures are illustrated in Figure 2. They were named 3F6-a, 3F6-b, 5F6-a, 5F6-b, and 7F6-h, with -a referring to arrangements having side chains placed on the same side of the backbone, -b referring to alternate sides (-b), and -h referring to a helix-type structure. In Table 1, we also tabulated the dihedral angles between repeat units, calculated using the DFT method mentioned in section II, for each conformation investigated at the minimum energy.

The data displayed in Table 1 suggest that 3F6 (dihedral angle DA with ca. $\pm 123^\circ$) tends to be ordinarily twisted, while for 5F6-a, DA distributions were found at about $\pm 50^\circ$ ($\pm 5^\circ$), indicating that all aliphatic chains were positioned on one side of the backbone due to strong intermolecular repulsions. Planar conformations for 5F6-a are unavailable due to the onset torsion revealed by the theoretical results. We observed that the helical form appears after the fifth monomer. This behavior agrees well with the experimental helical structure observed in thin films reported in the literature.⁹ Moreover, we found a clear helical shape for the 7F6-a structure, and most dihedral angles of reference are negatives (ca. $-50^\circ \pm 5^\circ$). This

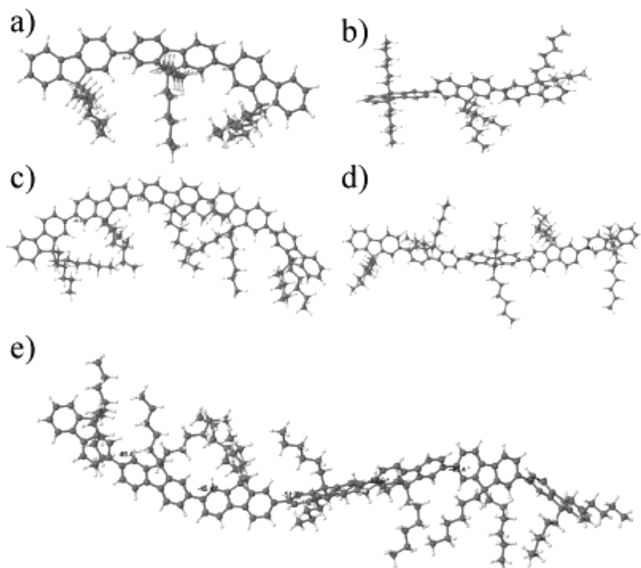


Figure 2. Selected chain conformations obtained for the investigated oligofluorenes: 3F6-a, 3F6-b, 5F6-a, 5F6-b, and 7F6-h, where -a and -b indicate arrangements with side chains on the same side (-a) or alternated (-b) with respect to the backbone, and -h indicates a helix-type structure. Other conformations tested are shown in Figure 2S of the Supporting Information.

Table 1. Dihedral Angles (deg) Obtained from DFT Calculations for Each Chain Arrangement at Energy Minima for Trimer, Pentamer, and Heptamer Oligomers

structures	dihedral angles					
	1	2	3	4	5	6
3F6-a	124°	-123°				
3F6-b	42°	-44°				
5F6-a	-42°	51°	-50°	56°		
5F6-b	143°	155°	-125°	-131°		
7F6-a (helical)	46°	-45°	-52°	-53°	-45°	-57°

conformation is in agreement with the X-ray and electron diffraction measurements for poly(2,7-fluorene)s reported by Scherf et al.,¹⁷ who found a helical conformation for poly(9,9-n-diethyl-fluorene). The rotational potential of the backbone favors a typical helical conformation. In addition, it is no longer possible that 7F6 exhibits branches located on the same side of the backbone without considering neighborhood forces, for example, packing, due to strong intermolecular repulsions, which induce natural distortions in the chains. Even when we impose an initial conformation for all of the alkyl branches, which are on the same side, we find that the final geometry clearly shows a tendency to be twisted.

UV–Vis Electronic Absorption: Theoretical and Experimental. The next step was to theoretically obtain the UV–vis spectra. The calculated spectra for 3F6, 5F6, and 7F6 conformations depicted in Figure 2 are shown in Figure 3a–d. Figure 3e presents the spectra calculated without aliphatic (C_6H_{13}) side chains. We observed that aliphatic side chains located at the C-9 position in the cyclopentadiene of fluorene induced a red shift in the main bands. On the other hand, the sequence of the bands does not change. The calculated spectra differ from the experimental measurements (Figure 3f) in the width of the bands. It is important to remark that the effects of solid-state molecular packing and conformational disorder

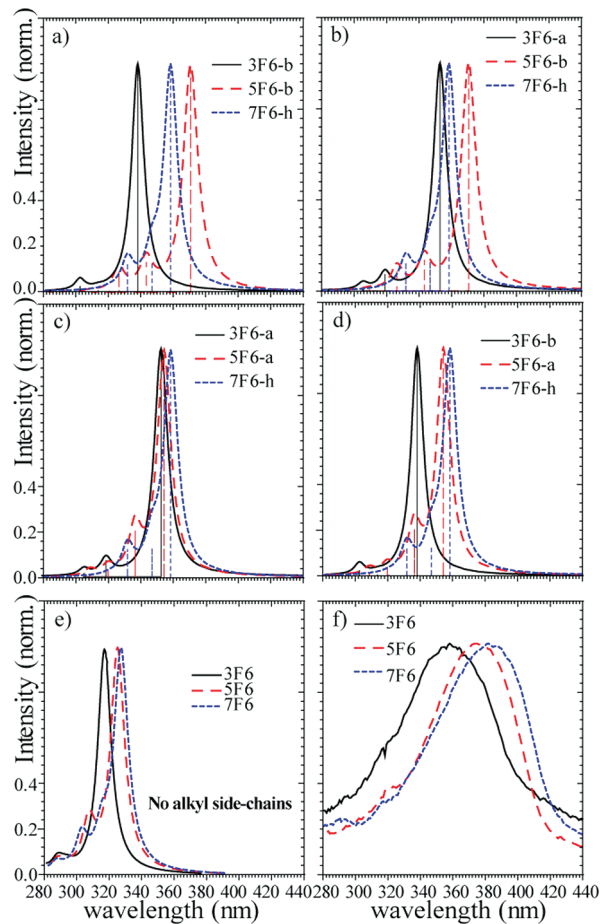


Figure 3. UV–vis theoretical and experimental UV–vis spectra of 3F6, 5F6, and 7F6. (a–d) Theoretical UV–vis spectra considering combinations of the side-chains arrangements shown in Figure 2. (e) Theoretical UV–vis spectra considering the conformation calculated without side chains. (f) Experimental spectra for the solid-state films.

broaden the absorption bands¹⁸ and also induce a red shift. Table 2 displays the results of the maximum absorption

Table 2. Maximum Wavelengths Obtained from Theoretical and Experimental UV–Vis Bands^a

structures	theoretical maximum wavelength λ_{teo} (nm)	experimental maximum wavelength λ_{exp} (nm)	difference $(\lambda_{\text{7F6}} - \lambda_{\text{exp}})$ (nm)	difference $(\lambda_{\text{7F6}} - \lambda_{\text{teo}})$ (nm)
3F6-b	338	358 ± 3	20	24 ± 6
5F6-a	354	375 ± 3	4	7 ± 5
7F6-h	358	382 ± 3	0	0

^aTheoretical data were calculated for different backbone arrangements of trimer (3F6-a and 3F6-b), pentamer (5F6-a and 5F6-b), and heptamer oligomers.

wavelengths for both the theoretically calculated and experimental results, and a comparison between them is shown on the basis of the difference relative to the 7F6 oligomer. Because we observed a good agreement between the calculated and measured spectra, we concluded that the best conformation is 3F6-b for the trimer, 5F6-a for the pentamer, and 7F6-h for the heptamer. This comparison is reinforced by

the similar values of the difference between the wavelengths ($\lambda_{7F6} - \lambda_{\text{teo}}$) and ($\lambda_{7F6} - \lambda_{\text{exp}}$), as shown in Table 2.

¹³C NMR: Theoretical and Experimental. Conformational changes in a π -conjugated system modify the local magnetic field experienced by carbon nuclei, which is reflected in the corresponding chemical shifts. This effect makes ¹³C NMR particularly sensitive to backbone conformations. Thus, a different set of chemical shifts is possible for each structural arrangement, as a type of fingerprint of the chain conformations. To find more-probable conformations, theoretical ¹³C NMR spectra were calculated for each oligomer arrangement and compared to the experimental spectra, Figure 4a. Because the backbone carbons are the most sensitive to

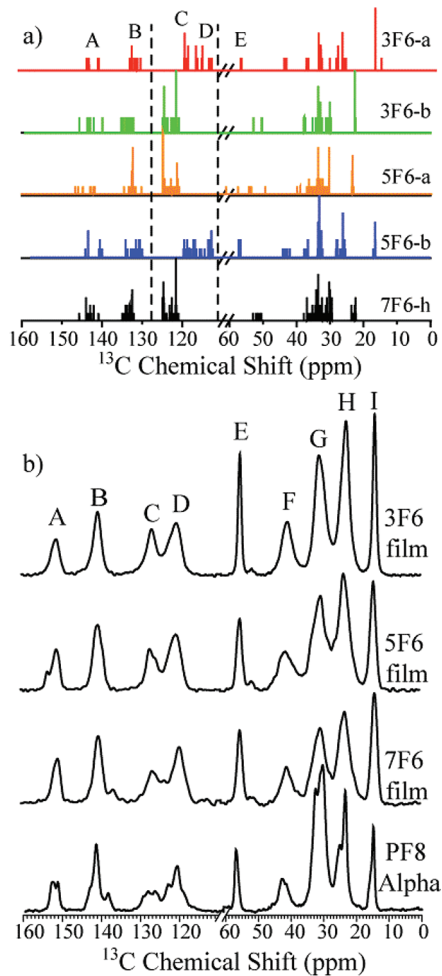


Figure 4. (a) Theoretical ¹³C NMR spectra calculated for five structural arrangements. (b) ¹³C CP-MAS solid-state NMR spectra of (from top to bottom) 3F6, 5F6, 7F6, and PF8.

conformational changes, the ¹³C NMR resonances associated with the backbone carbons were grouped into five sets: A, B, C, D, and E. The assignments were done using the carbon numbering of Figure 1a. The A set is associated with carbon 6 of fluorene rings. They are located in the 140 ppm region. The B-set peaks are related to carbons 5 and 7, clustered approximately 133 ppm. The C and D sets belong to carbon 3 (119 ppm) and 2 and 4 (close to 116 ppm), respectively. Near 57 ppm, we found the E set, related to the carbon assigned as 1 belonging to the five-ring tip of fluorene. Comparisons between these spectra for each structural

arrangement studied show that the most significant shift occurs for groups C and D, indicated by dashed lines in Figure 4; the same holds for the group E peaks with respect to the helical structure (7F6-h). Particularly, it is evident that for the conformations 3F6-a and 5F6-b, the sets of peaks C and D are shifted downfield.

Figure 4b shows the ¹³C CP-MAS spectra for films of the three oligomers and, for comparison, the spectrum of a polyfluorene (PF8) in the α crystalline phase.^{9,19,20} As shown, the line patterns for the backbone have the same structure as the theoretical spectra, composed of the lines A, B, C, D, and E. Moreover, four side-chain lines indicated as F, G, H, and I are observed. On the basis of their chemical shift values, these lines can be assigned as follows: line F, carbon 8; line G, carbons 9 and 10; line H, carbons 11 and 12; line I, carbon 13. In general, the spectra are similar for all oligomers and the polymer, which is expected due to the same chemical composition shared by the materials. Despite this similarity, the backbone lines show specific features for each oligomer, with the presence of extra lines and/or shoulders, which can be attributed to different chain conformations. Specifically, one can notice that the 3F6 spectra are almost homogeneously broadened, suggesting a random backbone conformation.²¹ For the 5F6 and 7F6 spectra, the backbone lines are clearly split, indicating the presence of chains with defined conformations. The spectra of PF8 in Figure 4b show clear similarity with the 7F6 spectra. The PF8 sample used to acquire these spectra was chloroform-cast and thermally annealed at 433 K, followed by slow cooling to room temperature. According to the literature,⁹ this produces an α -phase, in which the backbone conformation is helical. This finding was confirmed by X-ray diffraction of the sample. Therefore, the similarity between 7F6 and PF8 suggests that a considerable part of the heptamer chain has a helix-like conformation, although with a higher distribution in torsion angles than in PF8. The independent observation of helix-like conformations in the 7F6 films supports the use of this oligomer as a reference for interpreting the UV-vis absorption results.

In comparing the conditions of the systems (vacuum and single molecules) used in the theoretical models to those of the solid-state experimental sample, the exact values of the chemical shifts are not expected to match perfectly, but we could search for specific features that indicate the prevalence of a given conformation in the films. In this sense, the similar shape of the group C and D lines in the simulated spectra of 7F6 as compared to the experimental spectra reinforces the notion that chains with helix-like conformations exist in this sample. Moreover, by comparing lines C and D in the experimental spectra, we observe that they lie in the same spectral region; that is, there is no relative shift, which, based on the theoretical results, indicates that the conformations 3F6-b, 5F6-a, and 7F6-h are most likely to be present in the films. This result is also in agreement with the random-chain conformation for 3F6 because the structure 3F6-b (dihedral angle with ca. $\pm 123^\circ$) tends to be ordinarily twisted, and we presume that the material based on this structure will most likely be disordered.

Effects of Thermal Treatment on the Chain Conformations. It is well-known that thermal treatments have strong effects on the molecular packing and chain conformation of conjugated systems. This effect occurs because the tendency of structures to adopt a preferential chain conformation may dictate a specific molecular packing, which can be strengthened by thermal treatments. Once we observed that each oligomer

adopts a distinct conformation in the as-cast films, it was worth investigating the effect of thermal treatment on the chain conformation. This was achieved by analyzing the effect of temperature on the ^{13}C CP-MAS NMR spectra, which was shown to be quite sensitive to specific chain conformations (Figure 4). Hence, we performed NMR measurements as a function of temperature by following the procedure described in the Experimental Procedures.

Figure 5a shows the solid-state ^{13}C CP-MAS spectra at selected temperatures for the 3F6 oligomer. From bottom to

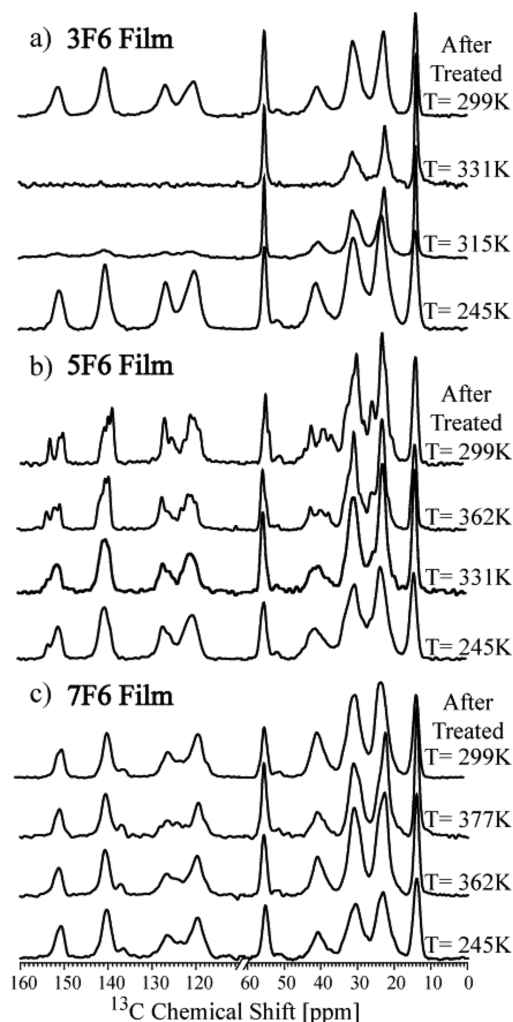


Figure 5. Solid-state ^{13}C CP-MAS spectra at selected temperatures obtained during the thermal treatment described in the Materials and Methods. From bottom to top, the first three spectra were obtained during sample heating, while the fourth was obtained after sample cooling. (a) 3F6, (b) 5F6, and (c) 7F6.

top, the 3F6 spectra depicted in Figure 5a show that the intensities of the backbone lines are drastically reduced above 315 K, disappearing at 331 K. It is known²² that the polarization transferred between rich and rare nuclei (^1H - ^{13}C) depends on the presence of dipolar coupling between them. In particular, isotropic molecular dynamics with rates in the 1–10 kHz range prevents cross-polarization, especially for longer contact times.²² Molecular movements in this dynamical range also interfere with the ^1H decoupling, broadening the ^{13}C signals.²¹ Thus, the disappearance of the backbone signal in the 3F6 film indicates the onset of molecular

motions at a rate on the order of 10 kHz. In other words, the sample undergoes a transition to an isotropic melt at this temperature. Together with the random conformation at low temperature, this shows that the 3F6 films undergo a transition from an amorphous glass to an isotropic liquid between 245 and 315 K. This is in agreement with the phase diagram for oligofluorenes (similar to those studied here, nevertheless with an ethyl ramification in the side chain) reported by Wegner et al.,^{23,24} who revealed a single transition from a glass to an isotropic liquid (T_g) at approximately 280 K for the corresponding trimer. Indeed, in ref 23, the average ^1H - ^1H dipolar coupling was also measured as a function of temperature, and the results show that at approximately 310 K the normalized H-H dipolar coupling is 0 on average; this also indicates that the onset of isotropic local reorientation occurs at rates longer than ~10 kHz at this temperature, in full agreement with the temperature dependence of the CP-MAS spectra reported here. After cooling from the isotropic melt state, the 3F6 film exhibited the same spectral response as that found initially (Figure 5a, top), showing that the thermal treatment during the NMR measurement had no significant effect on the conformational state of the oligomer chains.

Figure 5b shows the solid-state ^{13}C CP-MAS spectra at selected temperatures for the 5F6 oligomer. In this case, the spectral shape starts to change at 331 K, becoming remarkably distinct at 362 K. There is a clear splitting and narrowing of the lines, especially in the region related to the backbone. This behavior can be interpreted as a result of conformational change due to increasing chain ordering. In this respect, the phase diagram reported in ref 23 for the corresponding pentamer predicts two main transitions, from glass to liquid crystal (T_g) at approximately 320 K and from liquid crystal to isotropic liquid (T_{LC}) at approximately 410 K. In principle, one could tentatively assign the changes observed in the CP-MAS spectrum of the 5F6 film between 331 and 362 K to a glass-to-liquid-crystal transition. However, there are two remarkable features that made this interpretation dubious. The first is related to the featured lines observed at low temperature, which may be associated with the presence of defined conformations, that is, local ordering of the chains. The second is related to the higher definition and the increase in the CP-MAS signal intensity observed for the lines at temperatures above the transition temperature. Moreover, the same spectrum is observed after the slow cooling in the NMR rotor, suggesting that the highly ordered phase is frozen after the thermal treatment. All of these features would be more consistent with the presence of a solid-crystalline than of a liquid-crystalline phase.

Figure 5c shows the solid-state ^{13}C CP-MAS spectra at selected temperatures for the 7F6 oligomers. In this case, the spectral changes are more subtle than in the case of 5F6, but we see the appearance of shoulders in lines A, C, and D above 362 K, which become more evident at 377 K. Nevertheless, the appearance of new lines is not observed, which suggests that there is no emergence of a new solid-crystalline phase in the sample; however, it does suggest that there is a torsion-angle distribution of the chains. In this regard, this is consistent with the increase in the overall local chain ordering, possibly due to the formation of a liquid-crystalline phase as suggested in the literature.^{23–26} It is interesting that after cooling down (Figure 5c, top), the spectra become even more similar to the PF8 spectrum, confirming the presence of an organized phase in

which the chains adopt a conformation similar to that of the polymer.

To further study the phase behavior of the oligofluorenes, DSC measurements were carried out before (as-cast samples) and after the NMR measurements as a function of temperature (treated samples) (see the Materials and Methods section for details). The DSC thermograms for the as-cast 3F6 in both heating stages depict a single glass transition at about $T_g = 302$ K, confirming that the only transition in this sample is from a glassy to an isotropic liquid phase, as suggested by the NMR measurements. The DSC thermograms for the treated sample were quite similar, also indicating that there is no formation of significant crystalline phases during the NMR measurements (the small endothermic peaks appearing in the thermogram in the first sweep may be related to a very small portion of the ordered phase in the sample).

The DSC thermograms measured for the as-cast SF6 (Figure 6b) show two peaks in the first heating, which are related to melting at $T_m = \sim 329$ and ~ 420 K, and a broad exothermic band centered at approximately 380 K. The endothermic peak at 329 K has a heat of fusion of only 0.65 J/g and occurs just

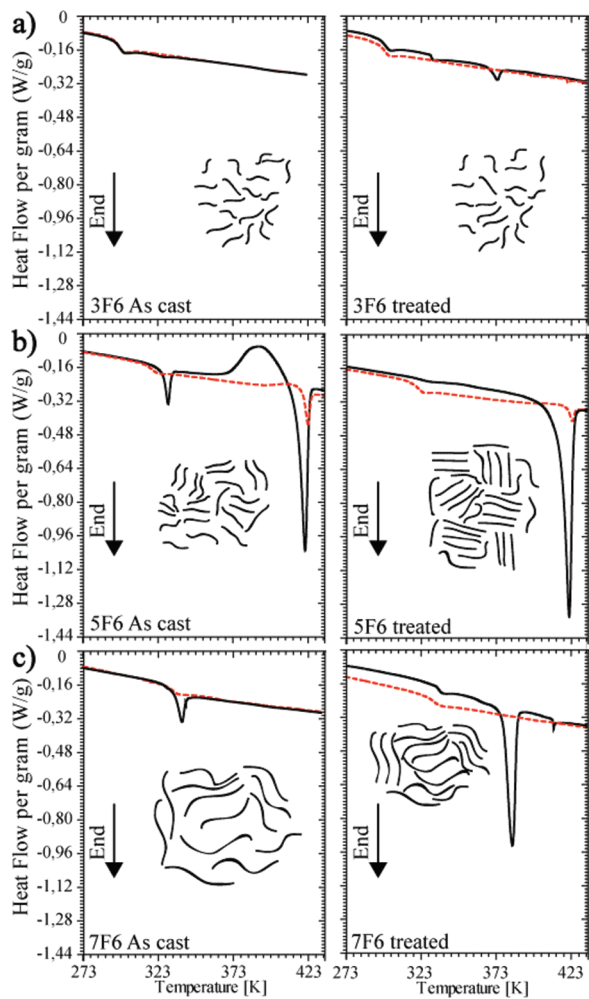


Figure 6. DSC thermograms measured for film samples of 3F6 (a), SF6 (b), and 7F6 (c) before (left) and after (right) the thermal treatment performed during the NMR measurements. The solid and dashed lines represent, respectively, the first and second DSC sweeps. A sketch of the sample morphologies, constructed on the basis of the NMR and DSC results, is shown in the inset.

beyond T_g . This type of behavior has already been observed for heptamer oligofluorenes films stretched over a polyimide substrate.²⁶ It was tentatively attributed to a reorientation relaxation effect due to the deformation or mechanical stress during quenching below the glass transition temperature. In this regard, because chloroform is a quickly evaporating solvent, it is likely that the same effect occurred at a molecular level even without physically stretching the samples. This finding is also in agreement with the line splitting observed in the CP-MAS NMR spectrum of the as-cast films. Indeed, if this small endothermic peak were a result of a small fraction of a solid-crystalline phase, the spectrum of the amorphous part would dominate, and a spectral shape more similar to that of 3F6 would be obtained. However, the most interesting feature in the DSC thermogram of the nontreated sample is the broad exothermic band that appears above 370 K. This can be attributed to a strong increase in molecular order, possibly due to the emergence of a more stable crystalline phase that melts at ~ 420 K. This is in good agreement with the NMR results, which clearly show a strong conformation change above 331 K. In the second heating, a glass transition at 323 K is readily observed, and the stable crystalline phase is not formed. Instead, a peak with a heat of fusion of 0.5 J/g is observed at 425 K. This is very similar to the results obtained for the heptamer in refs 23,24, where the heptamer was assigned a transition from a liquid crystal to an isotropic liquid. Therefore, these results suggest that solvent-induced chain ordering facilitates the crystallization of SF6. In the case of the treated sample, in addition to the glass transition at 323 K, an endothermic peak with a heat of fusion of 6.71 J/g is observed at 421 K. This finding indicates that the thermal treatment during the NMR measurements promoted the crystallization of the stable phase, which was retained after cooling the sample, and is also in accordance with previous NMR results. In the second heating stage, the typical behavior regarding the formation of a liquid-crystalline phase was also observed.

Figure 6c shows DSC thermograms measured for the as-cast 7F6 sample. In the first heating stage, we observe a melting peak at 339 K (heat of fusion of 9.88 J/g), while in the second heating step, a glass transition at about the same temperature is observed. This finding is also consistent with the previously reported results²⁴ and might additionally be related to reorientation relaxation effects. Contrary to the case of SF6, there is no formation of a new crystalline phase, and only a glass transition is observed in both heating stages. Indeed, according to refs 23,24, a LC–ISO transition would be detected only above 500 K. Interestingly, for the 7F6 treated sample, a melting peak with a fusion enthalpy of 3.77 J/g is observed at 383 K. However, one cannot exactly assign this peak; due to the temperature at which it appears and the associated heat of fusion, it does not seem to be related to an LC–ISO transition. Nevertheless, the similarity between the NMR spectrum of the as-cast film, the thermally treated film, and the crystalline α -phase of PF8 may be evidence that the thermal treatment induced the formation of an ordered phase in which the chains adopt a helical conformation.

The phase behavior of SF6 and 7F6, which produced some unique features in the NMR and DSC results, was further investigated by X-ray diffraction as a function of temperature. The 1D X-ray patterns at selected temperatures for the SF6 as-cast film are shown in Figure 7a. At low temperature, 123 K, a broad pattern with three maxima corresponding to characteristic lengths ($D_i = 2\pi/q_i$) of $D_1 = 13.9$ Å, $D_2 = 7.2$ Å, and

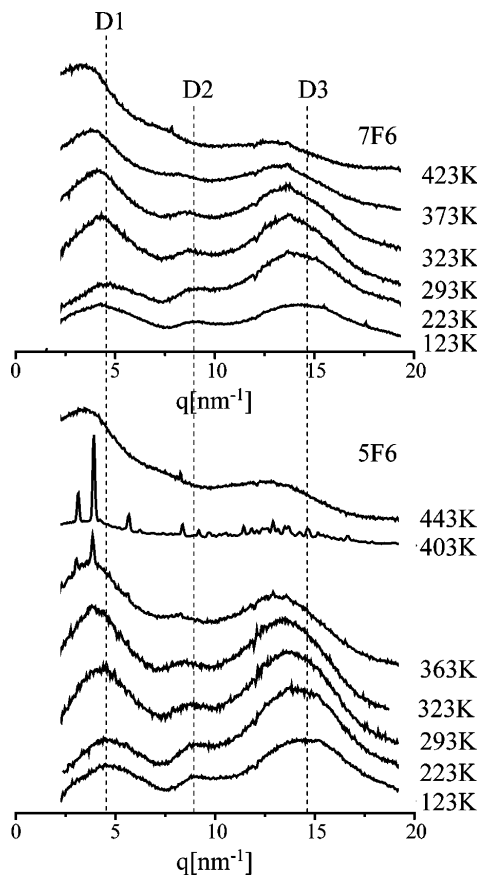


Figure 7. 1D wide-angle X-ray diffractograms at selected temperatures for the oligomers 5F6 (a) and 7F6 (b).

$D_3 = 4.5 \text{ \AA}$ suggests an aggregation structure similar to that observed in noncrystalline fluorene polymers^{27,28} and alkyl-side-chain-substituted PPV,²⁹ where the backbone rings are stacked parallel to each other with interplanar distances of 4.5 \AA and laterally spaced by the side chains with average distances of 13.7 \AA . The distance $D_2 = 7.2 \text{ \AA}$ is associated with the monomer length. At 293 K , the intensities increase and become sharper for the peaks corresponding to the characteristic lengths D_1 and D_3 , which also slightly shift toward low q values. Both features point to a slight change in local packing as a result of the orientation relaxation and the transition to a nematic LC phase, as suggested by the DSC measurements and reference.²³ However, the most remarkable feature in the X-ray results is the appearance of sharp lines above 363 K , which is associated with the appearance of a crystalline phase and is in full accordance with the change in the NMR ^{13}C CP-MAS line shape and the exothermal peak observed in the DSC. Indeed, the X-ray pattern at 443 K indicates that this phase melts between 403 and 433 K , which is also in agreement with the melting point observed in the DSC results, $\sim 420 \text{ K}$. Hence, the X-ray results for the 5F6 sample support the NMR and DSC results, pointing to the formation of a solvent-induced solid-crystalline phase for the pentamer and reinforcing the attribution of the low enthalpy melting peak at about T_g to an orientation relaxation effect. The 1D X-ray pattern of sample 7F6 as a function of temperature is shown in Figure 7b. The pattern is mostly identical to that observed for SF6, and the same line intensification, sharpening, and displacement is observed above 293 K . However, there is no appearance of sharp peaks, suggesting that despite a slight increase in molecular order,

there is no formation of a major crystalline in this sample, as suggested by NMR and DSC.

Effects of Chain Packing on Molecular Dynamics. The distinct packing behavior in each oligomer film leads to different morphologies, as discussed in the previous section. In addition to structural/morphological characterization, it is also interesting to infer how the different packing affects the chain dynamics. This can be achieved by solid-state NMR, which provides different methods that allow for the study of molecular motion over a wide frequency range, typically from hertz to megahertz.

The molecular dynamics in the oligomers chains was investigated using two specific NMR techniques dubbed dipolar chemical shift correlation (DIPSHIFT)³⁰ and center-band-only detection of exchange (CODEX).^{31,32} While DIPSHIFT is designed to probe molecular motions with rates within the kilohertz to megahertz range, CODEX is employed to detect and characterize slower motions with rates between hertz and kilohertz. In the temperature range studied herein, $250\text{--}400 \text{ K}$, we expected to observe molecular reorientations in the kilohertz to megahertz range in the oligomer side chains and conformation rearrangements at rates between the hertz and kilohertz range. Therefore, in this work, DIPSHIFT was used to probe side-chain motions, while CODEX was applied to investigate backbone motions.

As detailed in ref 30, the DIPSHIFT method provides a measurement of the $^{13}\text{C}-\text{H}$ magnetic dipolar coupling of each chemical group. This is achieved by measuring the dependence of the signal amplitude (each line in the CP-MAS spectrum) with an evolution period (t_1), where the nuclear spins evolve under the action of the CH magnetic dipolar coupling. This produces a curve $S(t_1)/S(t_1 = 0) = S(t_1)/S(0)$, which depends on the dipolar coupling strength. Motions with rates between $10^3\text{--}10^7 \text{ Hz}$ average the $^{13}\text{C}-\text{H}$ coupling, resulting in $S(t_1)/S(0)$ curves that depend on the presence of molecular motions. In the absence of molecular motions, the $S(t_1)/S(0)$ curves show typical behavior, decaying to a CH-coupling-dependent value when t_1 is one-half of the rotation period (t_r) and recovering to one when t_1 is equal to a full rotor period (rotational echo). If the molecular motion is isotropic and fast (with rates higher than $\sim 100 \text{ kHz}$), the dipolar coupling averages to zero and $S(t_1)/S(0)$ becomes equal to one. When the motion is fast but not isotropic, $S(t_1)/S(0)$ also decays at $t_1 = t_r/2$, but to a value that depends on the averaged CH coupling (residual CH coupling).

To probe the overall side-chain dynamics, the DIPSHIFT curves shown in Figure 8 were obtained from line G in the NMR spectra for the three studied oligomers at temperatures above and below the T_g values measured by DSC. In all cases, the motional averaging of the dipolar coupling is observed as the temperature increases. Nevertheless, while for 3F6 (Figure 8a) the motion tends to become isotropic above T_g (smaller residual dipolar coupling), in the case of 5F6 and 7F6 (Figure 8b and c), the curves indicate the presence of anisotropic motions in the side chains even above T_g . This finding is consistent with the presence of clustered side chains in the 5F6 and 7F6 samples, which is a consequence of the presence of ordered phases in these oligomers. This is confirmed by the curve obtained for 7F6 at $T = 383 \text{ K}$, which shows an extra averaging of the dipolar coupling.

The aforementioned side-chain motions are associated with secondary molecular relaxations, which are very common in branched polymers and oligomers. At temperatures above

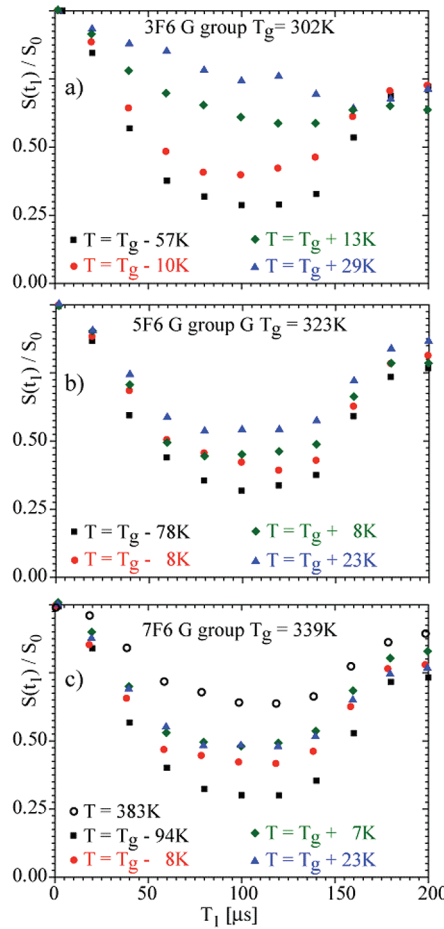


Figure 8. DIPSHIFT curves obtained at several temperatures (above and below T_g) for 3F6, 5F6, and 7F6 oligomers. The DIPSHIFT intensities $S(t_1)/S(0)$ were taken from line G in the ^{13}C NMR spectra to probe the overall molecular motion of the side chains. (a) 3F6, (b) 5F6, and (c) 7F6.

273 K, these motions become fast enough to be detected in a DIPSHIFT experiment. However, the experiments were unable to detect the presence of backbone motion even at temperatures around the glass transition temperature because the backbone motions are too slow to be detected in DIPSHIFT experiments. Thus, to probe backbone motions, we used the centerband-only detection of exchange (CODEX)³² in its variant form named constant time recoupling of the anisotropies (CONTRA). This experiment is capable of probing molecular motions with rates between hertz and kilohertz,³³ providing reliable information about the amplitude of the molecular motions. The experiment detects the signal reduction due to changes in the orientation-dependent chemical-shift frequencies (encoded by an evolution period with duration of $t_1 = s^*2t_r$, $s = 0,..,1$) that take place during a mixing time (t_m),³³ usually on the order of hundreds of millisecond. Quantification is performed by taking line intensities of the NMR spectrum obtained after applying the pulse sequence, S , and subtracting from the corresponding intensities obtained from a reference spectrum, S_0 . The reference spectrum is acquired in such a way that no molecular motion effects are encoded, but it has the same intensity reduction due to relaxation effects as the S spectra. The intensity difference obtained for each individual line in the spectra is then normalized, $\Delta S/S_0 = (S_0 - S)/S_0$, and plotted as

a function of t_m or t_1 , giving rise to a curve that depends on the correlation times (t_m dependence) or on the reorientation angle (t_1 dependence) of the slow molecular motion. Moreover, the asymptotic value of $\Delta S/S_0 = (S_0 - S)/S_0$, that is, t_m much higher than the correlation times ($t_m \gg \tau_c$) and t_1 much higher than the inverse width of the chemical shift anisotropy span ($t_1 \gg 1/\delta$), is proportional to the fraction of molecular segments that exhibit slow reorientation in the millisecond to seconds time scale. Strictly speaking, to precisely detect the motion amplitude, it is necessary to know the principal values and the principal axis orientation of the chemical shift anisotropy (CSA) tensor for the carbons used to probe the molecular motions. While the CSA principal values can be easily obtained using so-called Herzfeld and Berger analysis,³⁴ the determination of the principal axis orientation relative to the molecule is more problematic and, when possible, requires extensive multidimensional experiments.^{35,36} Hence, instead of trying to accomplish a profound characterization of the motion geometry, we focus on the general features concerning the motion of the oligomer backbone, for example, if the motions around T_g are isotropic or anisotropic and, in the second case, if reorientations occur with small or high angles. To accomplish that, a rough estimation of the PAS orientation is sufficient. Accordingly, we used the signals from carbons 5 and 7 (line B in the ^{13}C NMR spectra) to build up the CONTRA curves and approximate the PAS orientation to that of quaternary carbons in phenylene rings.³⁷ Thus, for the 5,7-carbons, the principal axis corresponding to the principal value σ_{zz} (z -axis) was assumed to be normal to the ring plane. The x -axis, corresponding to σ_{xx} , is along the 5–7 axes, and the y -axis, corresponding to σ_{yy} , is in the ring plane, 90° to the 5–7 axes. The σ_{xx} , σ_{yy} , and σ_{zz} values were obtained from a Herzfeld and Berger analysis of the spinning sidebands; the values found were 36, 160, and 230 ppm, respectively. Once these values are known, the curves can be simulated using a specific home-built program.³⁸

Figure 9a shows the t_m dependence of $\Delta S/S_0 = (S_0 - S)/S_0$ for the three studied oligomers at their respective glass transition temperatures. As expected, all average correlation times are similar (same motion regime), with the curves' plateaus being the most pronounced difference among them. Indeed, together with the CP-MAS measurements, the plateau value of almost 1.0 suggests again that almost all molecules execute isotropic backbone motions. On the other hand, one cannot be sure of the presence of anisotropic motions for the SF6 and 7F6 oligomers based only on the plateau value of the t_m curves because motions can have different characteristics in the phases of these samples.

Figure 9b shows the t_1 dependence of $\Delta S/S_0 = (S_0 - S)/S_0$ for the 3F6 oligomer (not thermal treated), together with simple simulations considering reorientations with different reorientation angles. As shown, the best match is for high reorientation angles, as is expected for isotropic motions. However, a much better fit is achieved when the curves are simulated by considering a distribution of reorientation angles according to a random-jump model.²¹ Although a random-jump model is not the best model for describing T_g motions in glassy systems,²¹ in CODEX-like experiments it has shown behavior similar to the most accepted isotropic rotation diffusion model.³⁸ Therefore, with the comparative analyses between all results, one can ensure that, under the sample preparation conditions used herein, we observed that the 3F6 was in the glassy state. The sample submitted to thermal

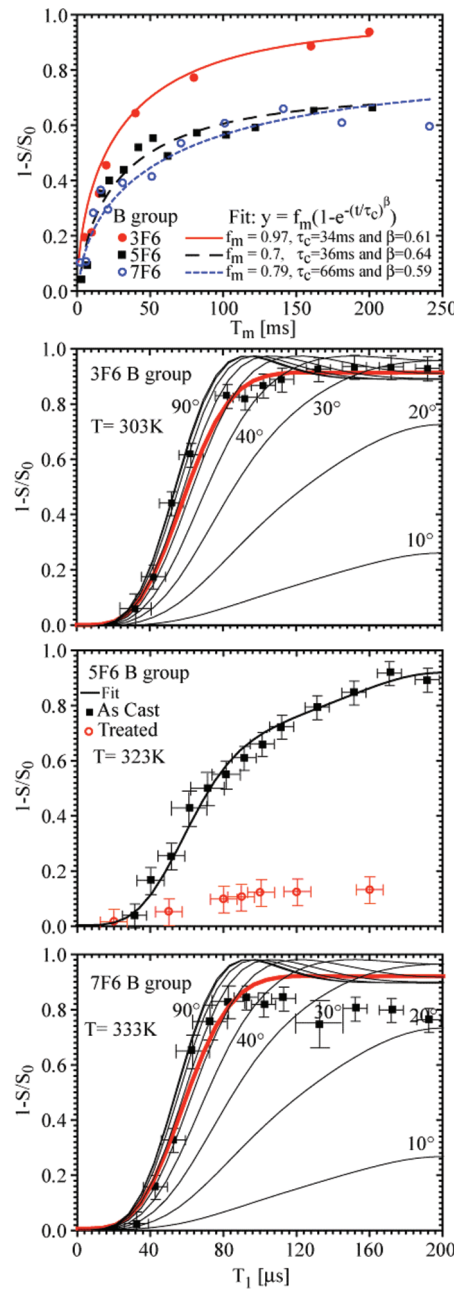


Figure 9. CONTRA $\Delta S/S_0$ curves obtained at temperatures around T_g for 3F6, 5F6, and 7F6 oligomers. In all cases, the line identified as G in the CP-MAS spectrum was used to obtain the CONTRA curves. (a) t_m dependence of $\Delta S/S_0$ for all three oligomers. (b) Experimental t_1 dependence of $\Delta S/S_0$ for 3F6 as-cast films together with simulations considering various reorientation angles or random-jump model.³⁸ (c) Experimental t_1 dependence of $\Delta S/S_0$ for the as-cast as well as for the thermally treated SF6 films and corresponding simulations. For as-cast films, the simulations consider a superposition of small-angle and isotropic motions, while for the treated films, the simulations correspond to small-angle librations of the backbone. (d) Experimental t_1 dependence of $\Delta S/S_0$ for 7F6 as-cast films together with simulations considering various reorientation angles or random-jump model.

treatment during the CP-MAS versus T measurements showed equivalent behavior.

Figure 9c shows the t_1 dependence of $\Delta S/S_0 = (S_0 - S)/S_0$ for the 5F6 oligomer (not thermal treated). In this case, we clearly see that the curves are bimodal, with a fast initial build

up followed by a slower one. This shows the presence of two phases with different dynamic behavior near the glass transition temperature. To confirm this, we performed a simulation in which we supposed that part of the sample executes random jumps (amorphous region) and another part executes reorientation by specific angles (conformational motions along the backbone). The fit is nearly perfect, considering that the conformational reorientations occur with rotation angles of approximately 19°. One should emphasize that the 19° angle is only a rough approximation because, due to the possibly misleading PAS orientations, this value can be different. Nevertheless, due to the high sensitivity of CONTRA to small-angle motions, one can still affirm that this reorientation angle is small, certainly smaller than 40°. It could be inferred that the as-cast 5F6 has two phases, a fully amorphous phase, in which the backbone executes isotropic reorientations at temperatures around T_g and a more ordered phase, in which only small-angle conformational reorientations occur. This again points to the association of the endothermic peak at T_g observed in the DSC measurement with an orientation relaxation effect. The t_1 dependence of $\Delta S/S_0 = (S_0 - S)/S_0$ for the 5F6 oligomer thermally treated during the CP-MAS versus T measurements is also shown in Figure 9c. The figure clearly shows that in this sample the slow backbone motions are drastically suppressed as a result of the increase in chain ordering and packing, confirming the presence of a solid-crystalline phase in this sample. Only very small-angle rotations remain, which, in principle, could be attributed to ring librations, but this cannot be assured because carbon driven spin diffusion can produce similar results.³⁹

Figure 9d shows the t_1 dependence of $\Delta S/S_0 = (S_0 - S)/S_0$ for the 7F6 oligomer (not thermal treated). Unlike that of 3F6, the curve does not seem to match to a fully isotropic motion; moreover, bimodal behavior (like that in 5F6) cannot be clearly observed. Because CONTRA is not sensitive to high-angle motions (Figure 3b) in the more ordered phase, the conformational motions might occur at high angles (consistent with a helical structure), and thus it becomes difficult to separate this contribution from the amorphous phase motions. Even after the thermal treatment, the curve does not change significantly, showing that the chain ordering in the 7F6 has a much a higher degree of disorder as compared to the 5F6 crystalline phase. However, it is not possible to prove this statement based only on a single CONTRA curve.

IV. DISCUSSION

Theoretical calculations showed that fluorene oligomers may adopt distinct conformations according to the number of monomeric units and that conformational changes modify the UV-vis spectra. We inferred that, in chloroform-cast films, 7F6 tends to adopt a distorted helical conformation, which is most likely associated with an ordered phase immersed in an amorphous phase. This notion was based on comparisons between the experimental and theoretical UV-vis and ^{13}C NMR results and on the similarity found between the 7F6 and the PF8 α -phase ^{13}C NMR spectra. NMR results indicate that the overall chain conformation of 7F6 oligomers thermally treated above T_g tends to be more well-defined. Moreover, the molecular dynamics studies showed that in this oligomer the side chains exhibit a significant motional hindrance even at temperatures above their glass transition temperature, once again suggesting the presence of more ordered regions in the

sample, possibly due to the formation of a liquid-crystalline phase above T_g as suggested in ref 23.

In the case of the 3F6 oligomer, it was found that the films studied did not form ordered phases, as evidenced by all results. In particular, we identified a glass transition in these materials using DSC and ^{13}C NMR, which disclosed that all of the molecular dynamics in this sample are consistent with the presence of a single disordered phase whose chains execute isotropic motions at temperatures around T_g .

In contrast, the 5F6 oligomer showed a strong tendency to crystallize, adopting a stable structure upon thermal treatment. The studies concerning the chain dynamics revealed the presence of hindered side-chain motions. What is more interesting is that by probing the slow backbone motion, we could infer the presence of a more-ordered phase in the as-cast 5F6 films, which is most likely associated with the endothermic peak around T_g observed in the DSC measurements. After the thermal treatment, the slow backbone motions were drastically suppressed as a result of the increased chain ordering and packing. A pictorial graph of this behavior is shown in the inset of Figure 7.

In summary, our results suggest that the helical conformation of 7F6 prevents the dense packaging of aliphatic branches, inducing conformational disorder. The small chain size of 3F6, added to the freedom exhibited by side chains, makes it more difficult to produce ordered phases with this oligomer. The distinct behavior of 5F6 can be understood by considering the tendency of this oligomer to adopt specific chain arrangements. In the more stable theoretical configuration of 5F6, the aliphatic side chains of different molecules can organize themselves into a more compact packing structure,⁴⁰ which explains the higher tendency to form a crystalline phase. It is important to mention that the use of different solvents and preparation procedures might induce the formation of other ordered phases, as was already described regarding the same type of oligomers documented in the literature.^{8,23,24,26} However, in all of the results reported thus far, 5F6 shows a higher tendency to crystallize than 3F6 and 7F6, suggesting that this is a solvent-independent behavior that is more associated with intrinsic intramolecular interactions, as suggested by our theoretical calculations.

V. CONCLUSIONS

This article presents an extensive theoretical and experimental study on the molecular structure and dynamics of chloroform-cast films of oligofluorenes with 3-, 5-, and 7-mers. On the basis of theoretical ab initio calculations, ^{13}C solid-state NMR, UV-vis electronic absorption, and DSC measurements, we conclude that, despite possible effects arising from solvent and film preparation, the oligomers exhibit a propensity to adopt specific chain conformations that dictate their packing behavior and consequently the tendency to crystallize or form ordered phases. In particular, we show that, while the heptamer tends to be helical, the pentamer chains have a tendency to organize their aliphatic side chains such that more-compact packaging can be obtained, which can be associated with the strong crystallization trend observed for this oligomer. Moreover, a more specific NMR study on the chain dynamics confirmed this finding regarding structure and explicitly shows the effect of chain packing on specific molecular motions at temperatures around the oligomers' glass transition.

■ ASSOCIATED CONTENT

■ Supporting Information

Figure 2S. This material is available free of charge via the Internet at <http://pubs.acs.org>.

■ AUTHOR INFORMATION

Corresponding Author

*E-mail: melissa.fsp@gmail.com (M.F.S.P.), azevedo@ifsc.usp.br (E.R.deA.).

Notes

The authors declare no competing financial interest.

■ ACKNOWLEDGMENTS

We are grateful to the Brazilian funding agencies FAPESP (Proc. number 2009/18354-8, 2007/08688-0), CAPES (Proc. number PNPD0052086), CNPq (Proc. number 579190/2008-0), and the National Institute of Science and Technology on Organic Electronics (INEO) for financial support and fellowships. We also thank the Brazilian Synchrotron Light Laboratory (LNLS) research proposal SAXS1-9208.

■ REFERENCES

- (1) Faria, G. C.; Plivelic, T. S.; Cossiello, R. F.; Souza, A. A.; Atvars, T. D. Z.; Torriani, I. L.; deAzevedo, E. R. *J. Phys. Chem. B* **2009**, *113*, 11403–11413.
- (2) Klaerner, G.; Miller, R. D. *Macromolecules* **1998**, *31*, 2007–2009.
- (3) Leclerc, M. *J. Polym. Sci., Part A: Polym. Chem.* **2001**, *39*, 2867–2873.
- (4) Yang, Z.; Hu, B.; Karasz, F. E. *J. Macromol. Sci., Part A: Pure Appl. Chem.* **1998**, *A35*, 233–247.
- (5) Takeda, N.; Asaoka, S.; Miller, J. R. *J. Am. Chem. Soc.* **2006**, *128*, 16073–16082.
- (6) Kadashchuk, A.; Schmeichel, R.; von Seggern, H.; Scherf, U.; Vakhnin, A. *J. Appl. Phys.* **2005**, *98*, 02410(1)–(8).
- (7) Zeng, G.; Yu, W. L.; Chua, S. J.; Huang, W. *Macromolecules* **2002**, *35*, 6907–6914.
- (8) Tsoi, W. C.; Lidzey, D. G. *J. Phys.: Condens. Matter* **2008**, *20*, 125213(1)–(8).
- (9) Chen, S. H.; Chou, H. L.; Su, A. C.; Chen, S. A. *Macromolecules* **2004**, *37*, 6833–6838.
- (10) Ponder, J. W. *Tinker - Software Tools for Molecular Design*, version 5.1; Ponder Lab, 2003.
- (11) Vila, J. A.; Baldoni, H. A.; Scheraga, H. A. *J. Comput. Chem.* **2009**, *30*, 884–892.
- (12) Zhang, Y.; Wu, A. N.; Xu, X.; Yan, Y. *J. Chem. Phys. Lett.* **2006**, *421*, 383–388.
- (13) Frisch, M. J.; Trucks, G. W.; Schlegel, H. B.; Scuseria, G. E.; Robb, M. A.; Cheeseman, J. R.; Montgomery, J.; Vreven, T.; Kudin, K. N.; Burant, J. C.; et al. *Gaussian 03*, revision B.4; Gaussian: Wallingford, 2004.
- (14) Neese, F. *ORCA - an Ab Initio, Density Functional and Semiempirical program package*; University of Bonn: Bonn, 2006.
- (15) Ridley, J. E.; Zerner, M. C. *Theor. Chim. Acta* **1976**, *42*, 223–236.
- (16) Bacon, A. D.; Zerner, M. C. *Theor. Chim. Acta* **1979**, *53*, 21–54.
- (17) Scherf, U.; List, E. J. W. *Adv. Mater.* **2002**, *14*, 477–487.
- (18) Winokur, M.; Slinker, J.; Huber, D. L. *Phys. Rev. B* **2003**, *67*, 184106(1)–(11).
- (19) Chen, S.; Su, A.; Su, C.; Chen, S. A. *Macromolecules* **2005**, *38*, 379–385.
- (20) Chen, S.; Su, A.; Su, C.; Chen, S. J. *Phys. Chem. B* **2006**, *110*, 4007–4013.
- (21) Schmidt-Rohr, K.; Spiess, H. W. *Multidimensional Solid-State NMR and Polymers*; Academic Press: San Diego, CA, 1994.
- (22) Cobo, M. F.; Malinakova, K.; Reichert, D.; Saalwachter, K.; DeAzevedo, E. R. *Phys. Chem. Chem. Phys.* **2009**, *11*, 7036–7047.

- (23) Somma, E.; Chi, C.; Loppinet, B.; Grinshtein, J.; Graf, R.; Fytas, G.; Spiess, H. W.; Wegner, G. *J. Chem. Phys.* **2006**, *124*, 204910(1)–(8).
- (24) Papadopoulos, P.; Floudas, G.; Chi, C.; Wegner, G. *J. Chem. Phys.* **2004**, *120*, 2368–2374.
- (25) Chi, C. Y.; Im, C.; Enkelmann, V.; Ziegler, A.; Lieser, G.; Wegner, G. *Chem.-Eur. J.* **2005**, *11*, 6833–6845.
- (26) Chi, C. Y.; Lieser, G.; Enkelmann, V.; Wegner, G. *Macromol. Chem. Phys.* **2005**, *206*, 1597–1609.
- (27) Chen, S. H.; Su, A. C.; Chen, S. A. *J. Phys. Chem. B* **2005**, *109*, 10067–10072.
- (28) Chen, S. H.; Su, A. C.; Huang, Y. F.; Su, C. H.; Peng, G. Y.; Chen, S. A. *Macromolecules* **2002**, *35*, 4229–4232.
- (29) Jeng, U.; Hsu, C. H.; Sheu, H. S.; Lee, H. Y.; Inigo, A. R.; Chiu, H. C.; Fann, W. S.; Chen, S. H.; Su, A. C.; Lin, T. L.; et al. *Macromolecules* **2005**, *38*, 6566–6574.
- (30) deAzevedo, E. R.; Saalwachter, K.; Pascui, O.; De Souza, A. A.; Bonagamba, T. J.; Reichert, D. *J. Chem. Phys.* **2008**, *128*, 104505(1)–(12).
- (31) deAzevedo, E. R.; Hu, W. G.; Bonagamba, T. J.; Schmidt-Rohr, K. *J. Am. Chem. Soc.* **1999**, *121*, 8411–8412.
- (32) deAzevedo, E. R.; Hu, W. G.; Bonagamba, T. J.; Schmidt-Rohr, K. *J. Chem. Phys.* **2000**, *112*, 8988–9001.
- (33) Reichert, D.; Pascui, O.; Bonagamba, T. J.; Belton, P.; Schmidt, A.; deAzevedo, E. R. *J. Magn. Reson.* **2008**, *191*, 141–147.
- (34) Herzfeld, J.; Berger, A. E. *J. Chem. Phys.* **1980**, *73*, 6021–6030.
- (35) Veeman, W. S. *Prog. Nucl. Magn. Reson. Spectrosc.* **1984**, *16*, 193–235.
- (36) Veeman, W. S. *Prog. Nucl. Magn. Reson. Spectrosc.* **1984**, *16*, 193–235.
- (37) deAzevedo, E. R.; Franco, R. W. A.; Marletta, A.; Faria, R. M.; Bonagamba, T. J. *J. Chem. Phys.* **2003**, *119*, 2923–2934.
- (38) Schmidt-Rohr, K.; deAzevedo, E. R. Bonagamba, T. J. *Encyclopedia of NMR*; John Wiley: Chichester, 2002; Vol. 9.
- (39) Reichert, D.; Bonagamba, T. J.; Schmidt-Rohr, K. *J. Magn. Reson.* **2001**, *151*, 129–135.
- (40) deAzevedo, E. R.; Bonagamba, T. J. *Braz. J. Phys.* **2006**, *36*, 61–74.